PHYSICAL REVIEW B, VOLUME 63, 134426

# Antiferromagnetic structure of $FePt_3$ films studied by neutron scattering

S. Maat, O. Hellwig, G. Zeltzer, and Eric E. Fullerton
*IBM Almaden Research Center, San Jose, California 95120*

G. J. Mankey
*University of Alabama, Tuscaloosa, Alabama 35401*

M. L. Crow and J. L. Robertson
*Oak Ridge National Laboratory, Oak Ridge, Tennessee 37831*

(Received 11 September 2000; revised manuscript received 4 December 2000; published 14 March 2001)

The magnetism of antiferromagnetic $Fe_xPt_{1-x}$ thin films ($x=0.27$ and 0.30) epitaxially grown onto MgO (110) and *a*-axis sapphire ($\alpha$-$Al_2O_3$) substrates has been studied by elastic neutron and x-ray scattering. Bulk chemically ordered $FePt_3$ exhibits an antiferromagnetic spin structure with a wave vector $Q_1=2\pi/a(\frac{1}{2}\frac{1}{2}0)$ below $T_{N1}\sim160$ K. For slightly Fe-rich alloys ($x\gtrsim0.26$) a spin-reorientation transition to a second antiferromagnetic phase with a wave vector $Q_2=2\pi/a(\frac{1}{2}00)$ occurs below $T_{N2}\sim100$ K at the expense of $Q_1$. For increased Fe content ($x\sim0.30$) the $Q_1$ phase is strongly suppressed with a dominant $Q_2$ phase. For (111)-oriented films grown on *a*-axis sapphire the spin structure is the same as that found in the bulk. The $x=0.27$ film exhibits transitions at $T_{N1}$ and $T_{N2}$. The film with $x=0.30$ exhibits an almost completely suppressed $Q_1$ phase and a dominant $Q_2$ phase with an enhanced ordering temperature of $T_{N2}\sim140$ K. In contrast $FePt_3$ (110) films grown onto MgO (110) exhibit only the $Q_1$ phase for both compositions $x=0.27$ and $x=0.30$ with the onset of the $Q_2$ phase suppressed. The distinct behavior of the films grown onto MgO from those grown onto *a*-axis sapphire and bulk $FePt_3$ may be explained by higher strain and defect densities incorporated in the films grown onto MgO.

DOI: 10.1103/PhysRevB.63.134426 PACS number(s): 75.50.Ee, 61.12.−q, 75.25.+z

## I. INTRODUCTION

The physics of metallic alloys with composition $XPt_3$ (where X is a $3d$ element) is rich and full of surprises. The chemically ordered alloys crystallize in the cubic $L1_2$ structure and change from ferrimagnetic (X=Cr)[1–3] to ferromagnetic (X=Mn)[1,4] to antiferromagnetic (AF) (X=Fe)[5,6] and back to ferromagnetic (X=Co),[7,8] as X is varied across the row of $3d$ elements in the periodic table. In $CrPt_3$, the Pt moments are aligned antiparallel to the Cr moments; in $FePt_3$ the Pt atoms carry no moment and the Fe atoms form an antiferromagnetic lattice. In $MnPt_3$ and $CoPt_3$ the moments of Mn or Co and Pt are aligned parallel. The chemically disordered $XPt_3$ fcc alloys behave very differently: $CrPt_3$ and $MnPt_3$[3,4] are nonmagnetic while $FePt_3$[5,6,9] and $CoPt_3$ (Ref. 8) are ferromagnetic.

The physics of $FePt_3$ is of particular interest: The chemically disordered phase is ferromagnetic with Fe moments of $2\mu_B$, while the chemically ordered phase is antiferromagnetic and can exhibit two different types of AF order as depicted in Fig. 1. In the bulk, the appearance of these two AF phases depends strongly on the deviation from the ideal composition.[5,6] The $FePt_3$ phase is maintained in $Fe_xPt_{1-x}$ alloys for $0.22<x<0.41$.[10] Upon cooling, bulk $FePt_3$ develops AF order below $T_{N1}=160$ K, where the Fe moments order in alternating ferromagnetic sheets in the (110) planes (see Fig. 1). This transition is of second order. The AF unit cell is obtained by doubling the $L1_2$ unit cell along the $x$ and $y$ axis and the corresponding wave vector is of type $Q_1=2\pi/a(\frac{1}{2}\frac{1}{2}0)$. The moments carried by the Fe are $3.3\mu_B$, which is an exceptionally high value for a $3d$ transition metal. For bulk alloys with stoichiometric composition only AF ordering of type $Q_1$ is found.[5] For slightly Fe-rich alloys a first-order transition into a second magnetic phase occurs below $T_{N2}\sim100$ K. This phase orders in alternating ferromagnetic sheets in the (100) planes. The AF unit cell for this phase is obtained by doubling the $L1_2$ unit cell along the $x$ axis and the corresponding wave vector is of type $Q_2=2\pi/a(\frac{1}{2}00)$. Mössbauer studies found that the excess Fe atoms occupy face centers randomly and couple ferromagnetically with the nearest neighbor Fe atoms into the (100) sheets rather than forming ferromagnetic clusters, thus allow-

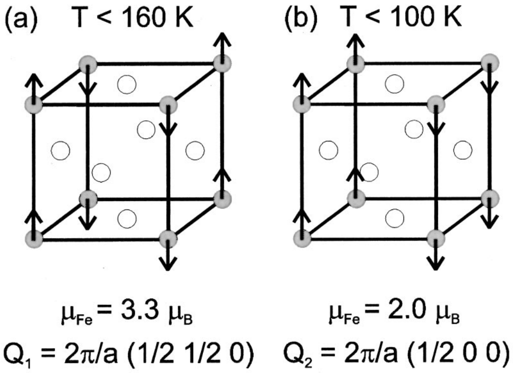

FIG. 1. The magnetic structure of $FePt_3$ in the $Q_1$ phase (a) and the $Q_2$ phase (b) are shown. The gray spheres represent the Fe atoms, which form a simple cubic lattice, and the white spheres represent Pt atoms.

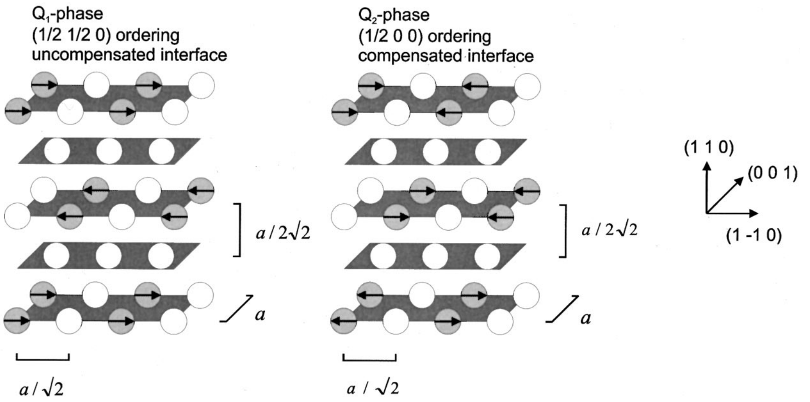

FIG. 2. Growing $FePt_3$ in the (110) direction results in either a spin-uncompensated interface for the $Q_1$ phase or a spin-compensated interface for the $Q_2$ phase (see Fig. 1). The gray spheres represent the Fe atoms; the white spheres represent Pt atoms. The atomic spacing and crystalline directions are indicated.

ing AF order to be maintained.[6] As in the disordered ferromagnetic phase the Fe atoms carry a moment of $2\mu_B$. The Pt sites are nonmagnetic for both $Q_1$ and $Q_2$ phases. In Fe-rich samples, the two AF phases coexist initially, however, the phase fraction of the AF $Q_1$ phase diminishes with further increase of the Fe content until it vanishes. Both neutron and Mössbauer measurements revealed that the $Q_1$ phase reorients into the $Q_2$ phase rather than forming a paramagnetic phase as the temperature is increased.[5,6]

The spin-wave dispersion spectra for the $Q_1$ phase have been measured by inelastic neutron scattering[11] and interpreted in terms of a simple Heisenberg model with localized Fe spins. Korringa-Kohn-Rostoker calculations identify nested electron and hole pockets at the $\Gamma$ and $M$ symmetry points of the simple cubic Brillouin zone of the paramagnetic state as being responsible for the $Q_1$ phase. These pockets are similar in size and shape and coincide after doubling the original simple cubic cell in the (100) and (010) directions. The $Q_2$ phase, however, is related to pockets at $\Gamma$ and $X$ although the nesting conditions are not as well fulfilled as for the $Q_1$ phase.[12,13]

In this work, we investigated the magnetism of chemically ordered epitaxially grown $FePt_3$ films. In particular we are interested in how epitaxial growth on different substrates will alter the spin reorientation observed for bulk $FePt_3$. Part of this work is also motivated by the potential use of $FePt_3$ as a model system for understanding mechanisms of exchange bias observed in AF-ferromagnetic bilayers. Exchange bias is a shift in the hysteresis loop of the ferromagnetic layer due to interfacial unidirectional exchange coupling to an adjacent AF layer. Growing $FePt_3$ single crystals in the (110) direction could result in spin-uncompensated or-compensated surfaces for the $Q_1$ and $Q_2$ phases, respectively, as shown in Fig. 2. This is independent of the spin axis of the Fe moments. This scenario is ideal for testing current models for exchange bias, which strongly depend on the AF moments at the interface.[14–17] By understanding the magnetic behavior of $FePt_3$ thin films, it may be possible to measure loop-shift and coercivity enhancement for two different types of interfaces in one sample by simply changing temperature and then relating the behavior observed to current models. In addition, because $FePt_3$ is ferromagnetic if chemically disordered, it may also be an ideal candidate for growing lattice-matched exchange coupled $FePt_3$(AF)/$FePt_3$(F) bilayers.

## II. EPITAXIAL GROWTH AND CHARACTERIZATION

Chemically ordered (110)- and (111)-oriented $FePt_3$ films were epitaxially grown simultaneously onto MgO (110) and $\alpha$-$Al_2O_3$ (11-20) substrates, respectively. To obtain the chemically ordered phase, the substrate was heated to 750 °C during deposition. The typical base pressure at this temperature was $2\times10^{-7}$ Torr. For comparison, the chemically disordered phase was grown under the same conditions, except that the substrate was heated to only 150 °C. A 1-nm-thick Fe layer followed by a ~2-nm-thick $CrPt_3$ layer was deposited prior to the deposition of the $FePt_3$ films. The Fe layer wets the MgO and we found that the $CrPt_3$ layer improves the crystalline orientation of the $FePt_3$ films on sapphire and suppresses growth of (100) impurity phases. 280-nm-thick alloy films were deposited by cosputtering Fe and Pt from dc-magnetron sources at an Ar pressure of 3 mTorr. Both $Fe_{27}Pt_{73}$ (denoted as $M1$ on MgO and $S1$ on $Al_2O_3$) and $Fe_{30}Pt_{70}$ (denoted as $M2$ on MgO and $S2$ on $Al_2O_3$) films were produced and characterized *ex situ*. The stoichiometry was determined within 1% uncertainty by Rutherford backscattering spectrometry and x-ray diffraction was used to analyze the chemical structure of the films. For the x-ray analysis we utilized a Philips X-pert x-ray spectrometer with a Cu cathode ($\lambda[K_\alpha]=1.54$ Å).

Figure 3 shows the out-of-plane $\theta$-$2\theta$ x-ray diffraction

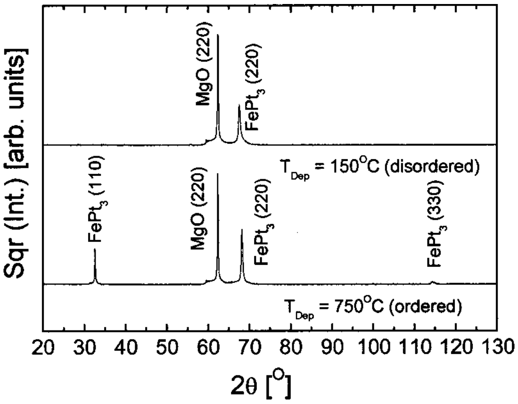

FIG. 3. Out-of-plane XRD spectra of $FePt_3$ films grown at 150 and 750 °C. The higher deposition temperature induced the chemically ordered phase as is evident from the otherwise forbidden (110) and (330) reflections.

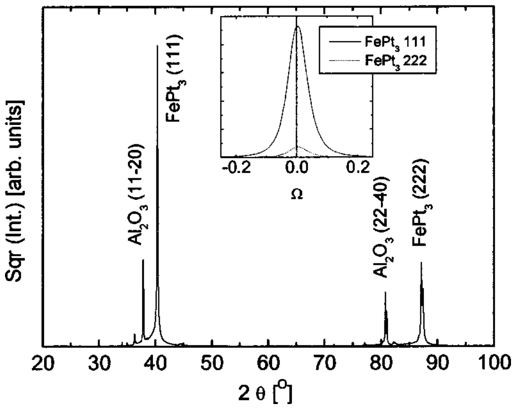

FIG. 4. Out-of-plane XRD spectrum of a 280-nm thick $FePt_3$ film grown at 750 °C on *a*-axis sapphire. The $FePt_3$ grows as a (111) bicrystal.

(XRD) scan along the surface normal of ordered and disordered $FePt_3$ (110) films grown onto MgO (110) substrates. Since the chemically disordered phase has cubic point symmetry and an fcc lattice, only the (220) fundamental peak is allowed. However, the chemically ordered phase has tetragonal point symmetry and an fcc lattice and thus (110) and (330) superstructure peaks are present. From the XRD spectra the out-of-plane lattice constant was determined to be $a = 3.882$ Å, slightly higher than for bulk $FePt_3$ (3.87 Å). To verify that the $FePt_3$ film was indeed a single crystal, pole figures were collected for various symmetry directions. The pole figures are very clean and show that only one crystalline orientation is present on MgO (110) substrates with the in-plane epitaxial orientation MgO[001]//$FePt_3$[001]. The in-plane lattice constants measured along the $[1\bar{1}0]$ and [001] directions are 3.853 and 3.866 Å, respectively. This indicates that the $FePt_3$ (110) films are distorted from there cubic symmetry. The full width at half maxima for the out-of-plane rocking curves of the (110) and (220) $FePt_3$ film peaks on MgO (110) were 0.89° and 0.57°, respectively. By comparing the integrated intensities of the (110), (220), and (330) rocking curves of the ordered $FePt_3$, the film was determined to be fully ordered in the $L1_2$ structure.

Figure 4 shows the out-of-plane $\theta$-$2\theta$ XRD scan for the ordered $FePt_3$ (111) film on sapphire. The out-of-plane lattice constants for $S1$ and $S2$ were determined to be 3.872 and 3.864 Å, respectively. For $S2$, the in-plane lattice spacing was determined to be 3.862 Å, suggesting that the $FePt_3$ samples on sapphire are essentially strain free. The rocking curve of the $FePt_3$ (111) peak shown in the inset of Fig. 4 determined an out-of-plane mosaic spread of only 0.04° indicating excellent crystal quality. Phi scans about the surface normal for the $FePt_3$ (110) and (220) (35.3° from the surface normal) and the $Al_2O_3$ (11-20) (60° from the surface normal) peaks, shown in Fig. 5, revealed that the $FePt_3$ grows in two bicrystalline orientations that are rotated 60° with respect to each other. The $FePt_3$ (11-2) axes of the bicrystals are rotated by ~6° relative to the in-plane *c* axis of the sapphire substrate. This rotational mode of strain relief was also observed for Nb and Mo on (11-20) $Al_2O_3$ (Ref. 18) and for Al on Si (100).[19] Assuming a rigid lattice and no strain relief the misfit for $FePt_3$[11-2]//$Al_2O_3$[0001] and $FePt_3$[110]//$Al_2O_3$[1-100] is

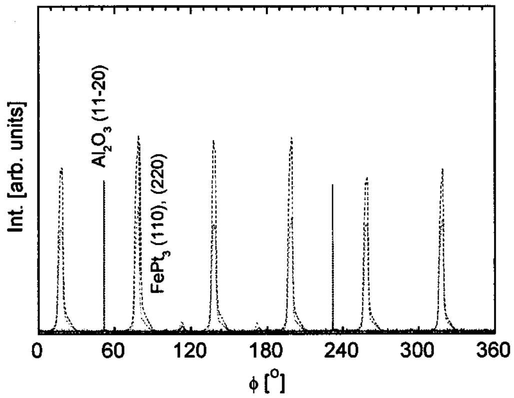

FIG. 5. Phi scans of the $FePt_3$ (110), (220) and the $Al_2O_3$ (11-20) reflections of a 280-nm thick $FePt_3$ film on *a*-axis sapphire. The scan reveals an ~6° rotation about the surface normal of the $FePt_3$ lattice relative to the sapphire lattice and is attributed to a rotational mode of lattice relaxation.

$$12 \cdot d_{(11\text{-}2)}(FePt_3)/d_{(0001)}(Al_2O_3) = 12.67\ \text{Å}/12.98\ \text{Å} \sim 0.98$$

and

$$4 \cdot d_{(110)}(FePt_3)/d_{(1\text{-}100)}(Al_2O_3) = 16.46\ \text{Å}/16.47\ \text{Å} \sim 1.$$

The rotation in only one direction may be caused by a slight miscut of the sapphire surface, which may energetically favor one rotational sense over the other. A sketch of the resulting measured pole figure is shown in Fig. 6.

The surface morphology of the films was checked by atomic force microscopy (AFM). A $500\times500\ \text{nm}^2$ scan of sample $M1$ is shown in Fig. 7(a). The root-mean-square (rms) roughness is 0.5 nm. The streaks that run diagonally across the image suggest (111) facets, which are often observed in fcc metals grown in the $\langle 110\rangle$ direction. A $5\times5\ \mu\text{m}^2$ scan of sample $S1$ is shown in Fig. 7(b). The surface shows ridges that are ~4 nm high and measure ~80 nm across. The surface between the ridges is very smooth with a rms of 0.7 nm. We attribute the ridges, absent in samples $M1$ and $M2$, as being either twin- or antiphase boundaries (APB's). The upper limit of the antiferromagnetic domain size should then be given by the typical distance between these boundaries, which is ~1 $\mu$m. APB boundaries in bulk $FePt_3$ (25.6% Fe) have been studied by transmission electron microscopy before.[9] Their average width was reported to be ~13 nm.

## III. NEUTRON SCATTERING

The AF ordering of the films was determined by elastic neutron diffraction measurements on beam-line HB1A ($\lambda = 2.357$ Å) at the High Flux Isotope Reactor at the Oak Ridge National Laboratory. The cross section of the neutron beam measured $2\times2$ cm, so that the samples were fully illuminated by the beam for all orientations. For cooling, the samples were mounted in a cryostat, which allowed

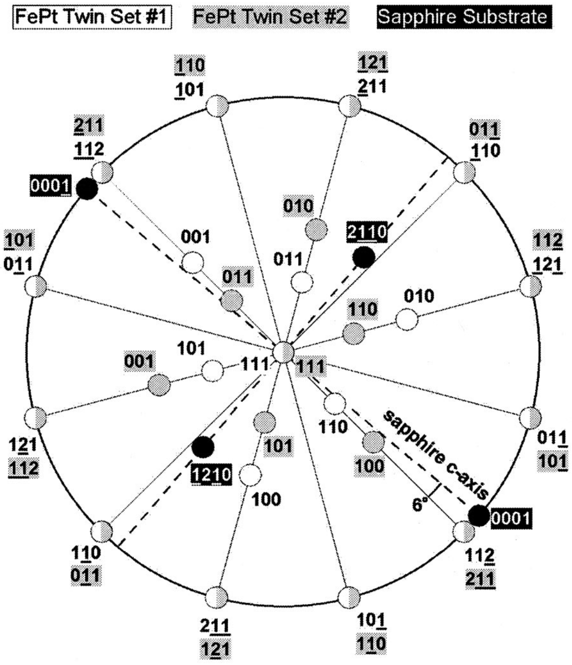

FIG. 6. Pole figure for $FePt_3$ on *a*-axis sapphire. Solid white and gray circles represent the $FePt_3$ directions of twins 1 and 2, respectively. Half-white and half-gray circles represent a direction common to twins 1 and 2. Solid black circles indicate the high symmetry directions of the sapphire substrate. The ~6° rotation of the $FePt_3$ with respect to the sapphire has been taken into account.

temperature-dependent measurements in the range of 10–300 K.

Although all the samples investigated are chemically ordered, unlike with x rays, chemical superlattice lines of the type (100) and (110) are not measurable with neutrons, since Fe and Pt have almost the same coherent scattering length for neutrons (9.45 and 9.60 fm, respectively).

### A. MgO substrates

For both films ($M1$ and $M2$) grown onto MgO (110), only ordering in the $Q_1$ phase was found below 160 K. The samples were examined for the $Q_2$ phase by searching for the presence of the magnetic $\langle \frac{1}{2}\ 0\ 0\rangle$ reflections, which were observed in Fe-rich bulk $FePt_3$.[5,6] Both the in-plane $[0\ 0\ \frac{1}{2}]$ and the $[\frac{1}{2}\ 0\ 0]$ reflections, 45° from the surface normal, were present in neither the $Fe_{27}Pt_{73}$ nor the $Fe_{30}Pt_{70}$ films at any temperature. Neither sample exhibited a magnetic $\langle \frac{1}{2}\ \frac{1}{2}\ \frac{1}{2}\rangle$ reflection.

The temperature dependent scattering intensities of the in-plane magnetic $[\frac{1}{2}\ -\frac{1}{2}\ 0]$ and out-of-plane $[\frac{1}{2}\ \frac{1}{2}\ 0]$ reflections were measured. Both peaks originate from a given domain state of the $Q_1$ phase. Both the in-plane and the out-of-plane AF peaks vanished at ~160 K in each sample, which is in agreement with the Néel temperature of bulk $FePt_3$.

Due to resolution limitations of the instrument, only a lower limit for the magnetic domain sizes in samples $M1$ and $M2$ could be determined from the width of the magnetic peaks: the magnetic domains in both samples are at least 100 nm in size at all temperatures.

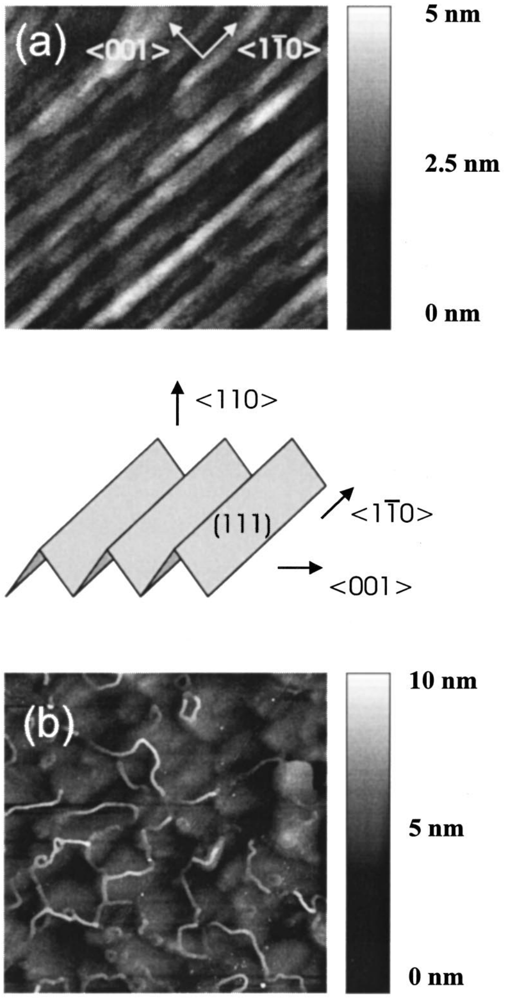

FIG. 7. (a) $500\times500\,\mathrm{nm}^2$ topographic AFM image of sample $M1$-$Fe_{27}Pt_{73}$ (110) grown at 750 °C onto MgO (110). The stripes indicate (111) facets, typical for (110) epitaxial films. The rms roughness is 0.5 nm. (b) $5\times5\,\mu\mathrm{m}^2$ topographic AFM image of sample $S1$-$Fe_{27}Pt_{73}$ (111) bicrystal grown at 750 °C onto $Al_2O_3$ (11-20). The surface shows ridges, that are ~4 nm high and ~80 nm wide. The rms of the surface between the ridges is 0.7 nm. The stripes that run diagonally across the picture are parallel to the $Al_2O_3$ *c* axis.

Figures 8(a) and 8(b) show the temperature dependent integrated scattering intensities of the out-of-plane $[\frac{1}{2}\ \frac{1}{2}\ 0]$ and the in-plane $[\frac{1}{2}\ -\frac{1}{2}\ 0]$ AF peaks of samples $M1$ and $M2$, respectively. The integrated intensity was corrected for background by subtracting an identical scan collected at 220 K, which is well above the Néel temperature, from low-temperature $q$ scans. The $[\frac{1}{2}\ \frac{1}{2}\ 0]$: $[\frac{1}{2}\ -\frac{1}{2}\ 0]$ ratio of the integrated scattering intensities (out-of-plane: in-plane) for samples $M1$ and $M2$ are plotted in Fig. 8(c). The ratios are ~0.5 for $M1$ and ~0.8 for $M2$ and are nearly temperature independent. We compared these intensities to the out-of-plane $[2\ 2\ 0]$ and the in-plane $[2\ -2\ 0]$ scattering intensities of the MgO in order to correct for geometric effects. The $[2\ 2\ 0]$: $[2\ -2\ 0]$ ratio of the MgO peaks was 1.5 for both samples, so the corrected ratios are further decreased to ~0.33 for $M1$ and ~0.53 for $M2$ after correction.

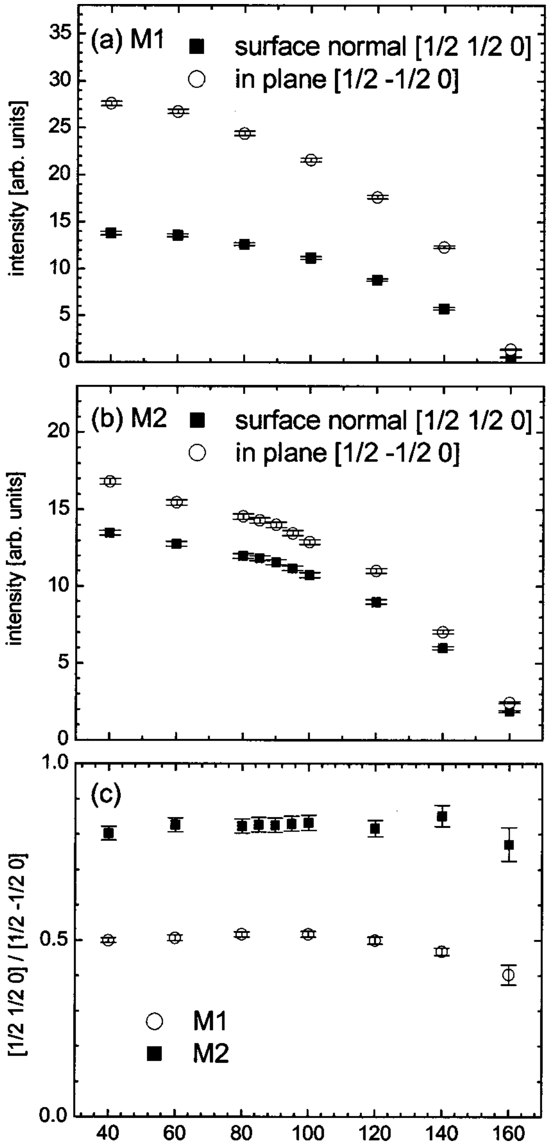

FIG. 8. (a) $[\frac{1}{2}\,\frac{1}{2}\,0]$ and $[\frac{1}{2}\,-\frac{1}{2}\,0]$ integrated intensities of sample $M1$. The in-plane $[\frac{1}{2}\,-\frac{1}{2}\,0]$ reflections are stronger than the out-of-plane $[\frac{1}{2}\,\frac{1}{2}\,0]$ reflections. (b) $[\frac{1}{2}\,\frac{1}{2}\,0]$ and $[\frac{1}{2}\,-\frac{1}{2}\,0]$ integrated intensities of sample $M2$. The in-plane $[\frac{1}{2}\,-\frac{1}{2}\,0]$ reflections are stronger than the out-of-plane $[\frac{1}{2}\,\frac{1}{2}\,0]$ reflections. (c) $[\frac{1}{2}\,\frac{1}{2}\,0]$: $[\frac{1}{2}\,-\frac{1}{2}\,0]$ integrated scattering intensity ratio for samples $M1$ and $M2$. The ratio is higher for $M2$ than for $M1$.

The direction of the spin axis of a single domain can be determined from the differences between the integrated intensities of symmetry equivalent magnetic reflections since only the component of the moments perpendicular to the scattering vector contribute to the observed intensity. For samples $M1$ and $M2$, the ratio of out-of-plane to in-plane scattering intensities is computed as

$$\frac{I[\frac{1}{2},\frac{1}{2},0]}{I[\frac{1}{2},-\frac{1}{2},0]}=\frac{\sin^2\Theta}{1-\sin^2\Theta\cos^2\Phi}, \tag{1}$$

TABLE I. The polar and azimuthal angles for spins lying in different high symmetry directions are listed in the second and third column, respectively. The theoretical out-of-plane to in-plane scattering intensity ratio is listed in the fourth column.

| *hkl* | $\Theta$ | $\Phi$ | $\frac{\sin^2\Theta}{1-\sin^2\Theta\cos^2\Phi}$ |
|---|---|---|---|
| $1\bar{1}0$ | 90° | 0° | ∞ |
| $1\bar{1}1$ | 90° | 35.26° | 3 |
| $\bar{1}11$ | 90° | 144.74° | 3 |
| 001 | 90° | 90° | 1 |
| 100 | 45° | 0° | 1 |
| 010 | 45° | 180° | 1 |
| 101 | 60° | 54.74° | 1 |
| $10\bar{1}$ | 60° | −54.74° | 1 |
| 011 | 60° | 54.74° | 1 |
| $01\bar{1}$ | 60° | −54.74° | 1 |
| 111 | 54.74° | 90° | $\frac{2}{3}$ |
| $11\bar{1}$ | 54.74° | −90° | $\frac{2}{3}$ |
| 110 | 0° | N.A.[a] | 0 |

[a] Not available.

where $\Theta$ and $\Phi$ denote the polar and azimuthal spin angles, respectively, and $\Theta$ is measured from the surface normal, i.e., the $[1\ 1\ 0]$ direction, and $\Phi$ is measured from the $[1\ -1\ 0]$ direction in the plane.

Bulk $FePt_3$ crystallizes in the cubic $L1_2$ structure and the spins are only allowed to point in high symmetry directions assuming a perfect crystal. The angles and the scattering ratios obtained from Eq. (1) for spins aligned along these high symmetry directions are listed in Table I. A (100) spin direction for the magnetic phases in bulk $FePt_3$ was suggested by diagrams in earlier publications on bulk $FePt_3$.[5,6] However, any (100) single or multiple domain state of (100) domains would yield an intensity ratio of 1, which is not observed here.

The fact that the in-plane intensity is higher than the out-of-plane intensity requires domains with a significant out-of-plane spin component [e.g., (110) domains]. Since the scattering intensity for the in-plane $[\frac{1}{2}\,-\frac{1}{2}\,0]$ reflections is higher for $M1$ than for $M2$ and the out-of-plane $[\frac{1}{2}\,\frac{1}{2}\,0]$ reflections are about the same for both $M1$ and $M2$, more spins in $M2$ have to be closer to the in-plane $[1\ -1\ 0]$ axis than in $M1$.

### B. $Al_2O_3$ substrates

The magnetic ordering for the $FePt_3$ on sapphire ($S1$ and $S2$) was found to be very distinct from the ordering on MgO and closer to that observed in bulk crystals. It is apparent from the pole figure in Fig. 6 that both twins contribute to the out-of-plane nuclear $[1\ 1\ 1]$ and all in-plane nuclear $[2\ -2\ 0]$ and magnetic $[\frac{1}{2}\,-\frac{1}{2}\,0]$ reflections. Sample $S1$ shows AF ordering in both the $Q_1$ and the $Q_2$ phases and behaves very much like bulk $FePt_3$. Since the $FePt_3$ grows as a bicrystal on sapphire both twins were measured [Figs. 9(a) and 9(b)]. The out-of-plane $[0\ \frac{1}{2}\ 0]$ and $[\frac{1}{2}\ 0\ 0]$ reflection of twins 1 and 2,

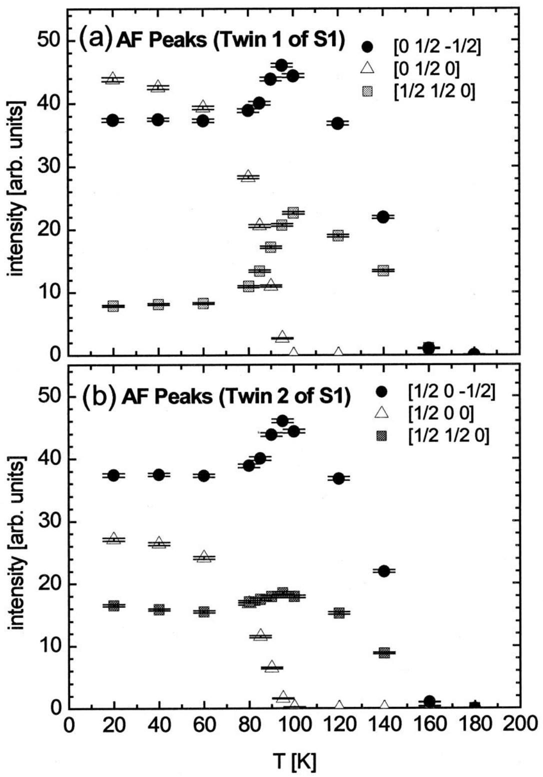

FIG. 9. (a) Magnetic peak intensities for the $[0\ \frac{1}{2}\ -\frac{1}{2}]$, $[0\ \frac{1}{2}\ 0]$, and $[\frac{1}{2}\ \frac{1}{2}\ 0]$ reflections from twin 1 of sample $S1$. (b) Magnetic peak intensities for the $[\frac{1}{2} 0\ -\frac{1}{2}]$, $[\frac{1}{2}\ 0\ 0]$, and $[\frac{1}{2}\ \frac{1}{2}\ 0]$ reflections from twin 2 of sample $S1$ (compare to diagram in Fig. 6).

respectively, decrease with temperature in a Brillouin function like manner and both vanish at $T_{N1}\sim 100\,\mathrm{K}$. The in-plane $[0\ \frac{1}{2}\ -\ \frac{1}{2}]$ and $[\frac{1}{2}\ 0\ -\frac{1}{2}]$ reflections, which originate from both twins and the out-of-plane $[\frac{1}{2}\ \frac{1}{2}\ 0]$ reflections of twins 1 and 2, exhibit a plateau at low temperatures, peak around $T_{N1}$, and vanish at $T_{N2}\sim 160\,\mathrm{K}$. The $\langle\frac{1}{2}\ \frac{1}{2}\ 0\rangle$ reflections are clearly suppressed upon the formation of the $Q_2$ phase at $T_{N2}$. An asymmetry between twin 1 and 2 is observed in the magnetic reflections: The peak exhibited by the $[\frac{1}{2}\ \frac{1}{2}\ 0]$ reflection of twin 2 is less pronounced than that by the $[\frac{1}{2}\ \frac{1}{2}\ 0]$ reflection and the $[0\ 0\ \frac{1}{2}]$ reflection of twin 2 is less intense than the $[0\ \frac{1}{2}\ 0]$ from twin 1. This indicates a higher volume fraction of twin 1 than twin 2 in this crystal. This asymmetry may be attributed to the 6° rotation of the $\mathrm{FePt_3}$ on the sapphire in only one sense.

Figure 10 shows the $[0\ \frac{1}{2}\ -\frac{1}{2}]$ and $[0\ \frac{1}{2}\ 0]$ intensities of twin 1 in the Fe-rich sample $S2$. For this sample the $Q_2$ phase is the dominant phase with the $[0\ \frac{1}{2}\ -\frac{1}{2}]$ reflection being almost entirely suppressed. However, a small amount of the $Q_1$ phase persists and its intensity peaks at ~120 K, where the $[0\ \frac{1}{2}\ 0]$ reflection has lost about half of its intensity, and maintains some intensity up to ~200 K as shown in the inset of Fig. 10. The $[0\ \frac{1}{2}\ 0]$ reflection is very strong and vanishes at $T_{N2}\sim 140\,\mathrm{K}$, a higher critical temperature than for sample $S1$. This increase of $T_{N2}$ with Fe content is consistent with bulk data.[5,6]

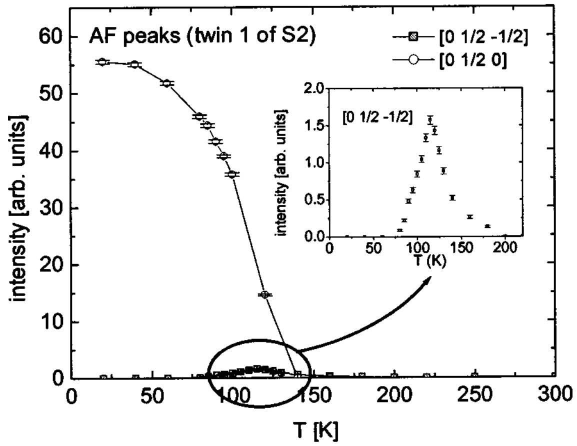

FIG. 10. $[0\ \frac{1}{2}\ -\frac{1}{2}]$ and $[0\ \frac{1}{2}\ 0]$ magnetic reflections of sample $S2$ (compare to diagram in Fig. 6). The temperature behavior of the $[0\ \frac{1}{2}\ -\frac{1}{2}]$ reflection, which is almost entirely suppressed, but peaks at ~120 K, is shown in the inset.

The width of the magnetic peaks in samples $S1$ and $S2$ was comparable to those in samples $M1$ and $M2$, so that 100 nm was also determined to be the lower limit for the magnetic domain sizes for $S1$ and $S2$ at all temperatures.

A correlation between chemical and magnetic peaks can be found for $S1$. The in-plane $[0\ 2\ -2]$ chemical peak [Fig. 11(a)] has a maximum at $T_{N2}=100\,\mathrm{K}$, where the magnetic $[0\ \frac{1}{2}\ 0]$ peak disappears. With increasing temperature, the intensity of the [2 2 0] and [0 2 0] chemical peaks [Figs. 11(b) and 11(c)] begin to grow at ~80 K, level at ~200 K, and remain constant up to room temperature. The nuclear [1 1 1] peak [Fig. 11(d)] decreases with increasing temperature and shows no correlation with the magnetic peaks. No anomaly was found in the chemical peak positions of sample $S1$. All

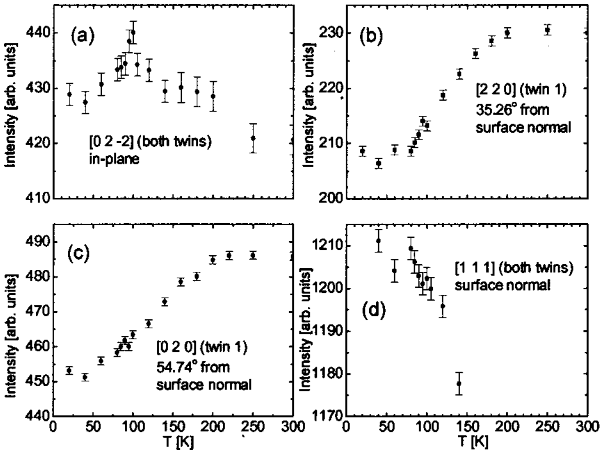

FIG. 11. Chemical peak intensities for sample $S1$: (a) the in-plane $[0\ 2-2]$ intensity peaks at 100 K, where the magnetic $[\frac{1}{2}\ 0\ 0]$ ordering disappears, (b) the [2 2 0] intensity, measured 35.26° from the sample normal, increases up to ~200 K, (c) the [0 2 0] intensity, measured 54.74° from the sample normal, increases up to ~200 K, and (d) the [1 1 1] intensity decreases monotonically with temperature.

chemical peaks shift monotonically to lower $q$, indicating an expansion of the lattice with increasing temperature.

The peak at ~100 K may be explained by spin frustration as the magnetic lattice goes through the spin-reorientation transition from the $Q_2$ to the $Q_1$ phase, in which case some of the Fe moments may align ferromagnetically and therefore give rise to a ferromagnetic contribution to the intensity of the in-plane chemical Bragg peak. Relating the anomalies in the chemical peaks to the spin-reorientation transition is supported by the observation that the chemical peaks in $S2$ are well behaved as are those of the $M1$ and $M2$ films on MgO. In these samples, the magnetic order is dominated by either the $Q_1$ or the $Q_2$ phase and the chemical peaks remain constant over the temperature range measured from 20 to 300 K.

Superconducting quantum interference device magnetometery was performed on samples $S1$ and $S2$ to investigate the magnetic behavior in more detail. In both samples, a small ferromagnetic signal can be measured and related to the magnetic ordering of the dominant AF phase. The samples were field cooled in a 20 kOe field and in-plane hysteresis loops for increasing temperature were acquired perpendicular to the in-plane $c$ axis of the sapphire. At 10 K after field cooling, sample $S1$ exhibits a coercivity of $H_C \sim 1.0$ kOe and a loop shift of $\sim -70$ Oe, and sample $S2$ exhibits a coercivity of $H_C \sim 4.1$ kOe and a small loop shift of $\sim -100$ Oe. Both the ferromagnetic component and the small exchange biasing had been observed in bulk samples.[5] Sample $S2$ is almost paramagnetic at room temperature, while $S1$ maintains some degree of ferromagnetic order. Hysteresis loops of sample $S2$ for four different temperatures are shown in Fig. 12(a). The temperature dependent coercivity of samples $S1$ and $S2$ is shown in Fig. 12(b) and 12(c), respectively and it is distinct from the behavior of uncoupled small Fe particles. The high coercivity suggests the presence of some ordered FePt rather than Fe particles or a strong coupling term between the Fe or FePt particles and the AF $FePt_3$ matrix.

Figures 12(d) and 12(e) show the remnant moment ($M_R$) of $S1$ and $S2$, respectively. $M_R$ decays with temperature and exhibits a plateau for sample $S2$ at ~100 K, where a small magnetic $(\frac{1}{2}\ 0\ \frac{1}{2})$ peak was observed by neutron scattering. The moment measured at 10 K is ~1% of the moment of bulk Fe for both samples, although $S2$ incorporates ~7% of excess Fe. The low moment supports the theory of excess Fe atoms preferentially occupying the face centers in the $L1_2$ unit cell rather than forming ferromagnetic Fe or FePt clusters.

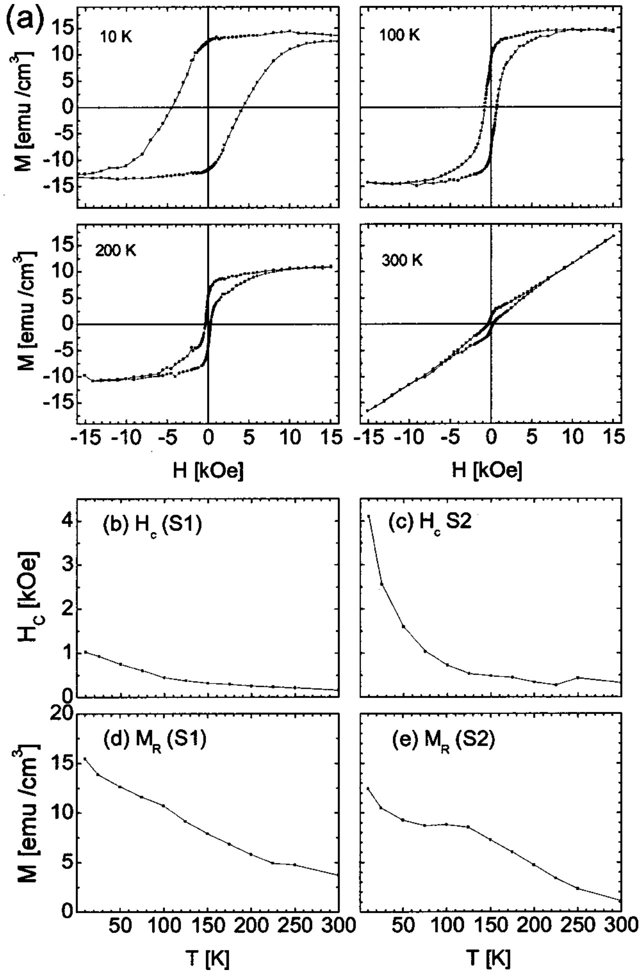

FIG. 12. (a) Hyteresis loops for different temperatures measured perpendicular to the in-plane $c$ axis of sample $S2$. The complete temperature dependence of the coercivity and remanent moment for samples $S1$ and $S2$ are shown in (b)–(d).

## IV. CONCLUSIONS

$FePt_3$ is a very simple AF system, since the Fe atoms are arranged on a simple cubic lattice. Nevertheless its magnetic properties are quite rich, since it exhibits two different kinds of AF ordering. We demonstrated that high quality epitaxial $FePt_3$ films can be grown onto MgO (110) and $a$-axis sapphire. Furthermore, we showed that substrate and film composition affects the AF ordering of $FePt_3$ thin films in a way not readily anticipated from the bulk data. For both $Fe_{27}Pt_{73}$ and $Fe_{30}Pt_{70}$ films on sapphire, the critical temperatures at which $(\frac{1}{2}\ 0\ 0)$ and $(\frac{1}{2}\ \frac{1}{2}\ 0)$ spin ordering occurs are the same as in bulk. However, we showed that $(\frac{1}{2}\ 0\ 0)$ ordering can be completely suppressed by growing $FePt_3$ onto MgO (110) and that $(\frac{1}{2}\ \frac{1}{2}\ 0)$ ordering can be suppressed by growing $Fe_{30}Pt_{70}$ onto $Al_2O_3$ (11–20).

The existence of a $Q_2$ phase in $S1$ and $S2$ may originate from the existence of twin and/or antiphase boundaries observed in bulk $FePt_3$ and films grown on sapphire. In these boundaries Fe can occupy Pt sites forming Fe-Fe next neighbor pairs. Those pairs couple ferromagnetically and spin frustration could be avoided by ordering exclusively in the $Q_2$ phase. For $Fe_{27}Pt_{73}$ on sapphire the magnetic $Q_2$ to $Q_1$ phase transition is reflected in some of the chemical Bragg peaks at ~100 K, which suggests additional ferromagnetic ordering due to spin frustration during the spin-order transition. The suppression of the $Q_2$ phase for $FePt_3$ films on MgO most likely results from strain and higher density of defects reflected in the larger x-ray rocking-curve widths.

The (110) films grown onto MgO(110) result in a spin-uncompensated surface, while the (111) bicrystals grown onto *a*-axis sapphire result in a spin-compensated surface. Although it was not possible to obtain both compensated and uncompensated surfaces within a single film at different temperatures, since the $Q_2$ phase is absent in MgO, the results presented here suggest that growing $FePt_3$ (110) on alternative substrates to minimize the strain could produce spin-compensated and-uncompensated surfaces in the same film. This would make $FePt_3$ an ideal candidate material to test current models of exchange bias. For this further understanding of the factors determining the spin configuration of $FePt_3$ alloy films is needed.

## ACKNOWLEDGMENTS

We would like to thank Andrew Kellock for the compositional analysis of our $FePt_3$ films and Robin Farrow for some helpful discussions on the epitaxial growth on sapphire. The Research of G.J.M. was sponsored by ARO Grant No. DAAH-04-96-1-0316 and shared equipment through NSF MRSEC Grant No. DMR-9809423. The research of J.L.R. was sponsored by the U.S. Department of Energy under Contract No. DE-AC05-00OR22725 with the Oak Ridge National Laboratory, managed by UT-Battelle, LLC.

---

[1] S. J. Pickart and R. Nathans, J. Appl. Phys. **34**, 1203 (1963).
[2] M. Maret, M. Albrecht, J. Köhler, R. Poinsot, C. Ulhaq-Bouillet, J. M. Tonnerre, J. F. Berar, and E. Bucher, J. Magn. Magn. Mater. **218**, 151 (2000).
[3] M. J. Besnus and A. J. P. Meyer, Physica B **55**, 521 (1973).
[4] B. Antonini, F. Lucari, F. Menzinger, and A. Paoletti, Phys. Rev. **187**, 611 (1969).
[5] G. E. Bacon and J. Crangle, Proc. R. Soc. London, Ser. A **272**, 387 (1963).
[6] D. Palaith, C. W. Kimball, R. S. Preston, and J. Crangle, Phys. Rev. **178**, 795 (1969).
[7] F. Menzinger and A. Paoletti, Phys. Rev. **143**, 365 (1966).
[8] M. C. Cadeville, C. E. Dahmani, and F. Kern, J. Magn. Magn. Mater. **54–57**, 1055 (1986).
[9] S. Takahashi and Y. Umakoshi, J. Phys.: Condens. Matter **2**, 2133 (1990).
[10] O. Kubschewski, *Iron-Binary Phase Diagrams* (Springer, New York, 1982).
[11] M. Koghi, Y. Ishikawa, and P. Radhakrishna, Solid State Commun. **27**, 409 (1978).
[12] N. I. Kulikov, J. Phys. F: Met. Phys. **15**, 1139 (1985).
[13] N. I. Kulikov, E. T. Kulatov, and S. I. Yakhimovich, J. Phys. F: Met. Phys. **15**, 1127 (1985).
[14] A. P. Malozemoff, Phys. Rev. B **35**, 3679 (1987).
[15] A. P. Malozemoff, J. Appl. Phys. **63**, 3874 (1988).
[16] T. C. Schulthess and W. H. Butler, Phys. Rev. Lett. **81**, 4516 (1998).
[17] T. C. Schulthess and W. H. Butler, J. Appl. Phys. **85**, 5510 (1999).
[18] D. M. Tricker and W. M. Stobbs, Philos. Mag. A **71**, 1037 (1995).
[19] F. J. Lamelas, M. T. Tang, K. Evans-Lutterodt, P. H. Fuoss, and W. L. Brown, Phys. Rev. B **46**, 15 570 (1992).